LAND COVER CHANGE MAPPING USING A COMBINATION OF SENTINEL-1 DATA AND MULTISPECTRAL SATELLITE IMAGERY: A CASE STUDY OF SANANDAJ COUNTY, KURDISTAN, IRAN

TIEN BUI, D.[1,2] – SHAHABI, H.[3*] – MOHAMMADI, A.[4] – BIN AHMAD, B.[4] – BIN JAMAL, M. H.[5] – NOOR MOHAMED, R. B.[5] – AHMADI, M.[6] – SHIRZADI, A.[7] – RAHMANI, H[8]. – PHAM, B. T.[9] – AHMAD, A.[4]

[1]Geographic Information Science Research Group, Ton Duc Thang University, Ho Chi Minh City, Vietnam

[2]Faculty of Environment and Labour Safety, Ton Duc Thang University, Ho Chi Minh City, Vietnam
(e-mail: buitiendieu@tdt.edu.vn)

[3]Department of Geomorphology, Faculty of Natural Resources, University of Kurdistan, Sanandaj, Iran

[4]Faculty of Built Environment and Surveying, Universiti Teknologi Malaysia (UTM), 81310 Johor Bahru, Malaysia
(e-mail: ayubmohammadi1990@gmail.com, baharinahmad@utm.my, anuarahmad@utm.my)

[5]School Civil Engineering, Faculty of Engineering, Universiti Teknologi Malaysia (UTM), 81310 Johor Bahru, Malaysia
(e-mail: mhidayat@utm.my, roslli@utm.my)

[6]Department of Geomorphology, Faculty of Geography and Planning, University of Tabriz, Tabriz, Iran
(e-mail: mehdi.ahmadi2009@gmail.com)

[7]Department of Rangeland and Watershed Management, Faculty of Natural Resources, University of Kurdistan, Sanandaj, Iran
(e-mail: a.shirzadi@uok.ac.ir)

[8]Department of Computer Science, Engineering and IT, School of Electrical and Computer Engineering, Shiraz University, Shiraz, Iran
(e-mail: hosein.rhm@gmail.com)

[9]Institute of Research and Development, Duy Tan University, 550000 Da Nang, Vietnam
(e-mail: phambinhgtvt@gmail.com)

**Corresponding author*
e-mail: h.shahabi@uok.ac.ir; phone: +98-918-665-8739

(Received 7th Dec 2018; accepted 28th Feb 2019)

Abstract. Land Cover Maps (LCMs) represent the integrated information about general status of a specific region, which are widely used as a baseline for many related purposes. This study aims to extract the land covers of Sanandaj County, Kurdistan, Iran, along with to highlight the occurred changes compared with an old map prepared by the Iranian Institute of Water and Soil in 2010. The combination model of Sentinel-1 and Landsat-8 satellite imageries was used for the dates 10/05/2017 and 11/05/2017, respectively. It is noted that based on the location of the study area we acquired Sentinel-1 data (S1A, IW,

http://www.aloki.hu ● ISSN 1589 1623 (Print) ● ISSN 1785 0037 (Online)
DOI: http://dx.doi.org/10.15666/aeer/1703_54495463

and GRD) and a pair of Landsat-8 images. Using Sentinel Application Platform (SNAP) and Environment for Visualizing Image (ENVI) softwares all images were corrected, co-registered and stacked. The combination of RADAR, NDVI and thermal bands was utilized as the best combination for the visual interpretation, with which all land covers can be easily differentiated. However, with help of the Google Earth images the land covers (polygon by polygon) were checked and digitized. Results indicate that the visual interpretation of the combination model with the assist of Google Earth is a robust way to extract land covers, provided that the researchers have enough knowledge on the land covers of the study area. This study can be applicable for decision makers of Sanandaj City.
Keywords: *Landsat, land use, remote sensing, Google Earth, GIS, Sanandaj*

Introduction

Land Cover (LC) is one of the most important factors that reflects the impacts of human on the environment (Belal and Moghanm, 2011; Lausch and Herzog, 2002), which it is constantly changing due to human activities (Chen et al., 2003). The importance of identifying, quantifying and supervising LCMs and their changes have widely been considered by the global and the regional studies (Jin et al., 2013; Kumar et al., 2016; Xian et al., 2009; Zhu and Woodcock, 2014). LC is a key factor, which affects the function and the condition of an ecosystem (El-Kawy et al., 2011; Hansen and Loveland, 2012; Lunetta et al., 2006). As a matter of fact, satellite based remote data have been widely employed as a robust and fast way to provide LC coverage in a large geographic scope (Grecchi et al., 2014; Li et al., 2017; Liu and Yang, 2015; Lunetta, et al., 2006; Myint et al., 2011). LCM studies and their monitoring using the combination of a few satellite imageries is greatly associated with the appropriate satellite images to evaluate the LC map (Liu and Yang, 2015; Lunetta, et al., 2006).

Understanding and identifying the human activities and LC changes' patterns are essential for the proper land management and sustainable development (Rawat et al., 2013; Rawat and Kumar, 2015). Regarding its impact on a natural ecosystem, the LCM is one of the main concerns of the conservationists, the environmentalists and the land cover planners (Halmy et al., 2015). Development of an appropriate analytical procedure and the techniques to map all the land covers in an area, is one of the main problems in LCMs (Hansen and Loveland, 2012; Xian, et al., 2009). Extracting land covers by using a combination of satellite images is normally faced a number of challenges, including acquisition of two or more satellite imageries at the regional or the national scales.

LCM provides the valuable information for a better understanding of the changes' mechanism on the environment (Boori et al., 2015; Xian and Crane, 2005; Xian, et al., 2009). Continuous, precise and up-to-date LC information is essential for the natural resources and the environmental management (Homer et al., 2004; Loveland et al., 2002; Rawat and Kumar, 2015; Xian, et al., 2009). Another significance of this study is the availability of both satellite imageries of RADAR (Sentinel-1) and multispectral (Landsat-8).

Many researches have been conducted with the LCM studies using a variety of techniques and imageries, including Markov-chain analysis (López et al., 2001), multiple regression analysis (Theobald and Hobbs, 1998), logistic regression (Wu and Yeh, 1997), artificial neural networks (ANNs) (Li and Yeh, 2002), cellular automata (CA) (Batty and Xie, 1994, 1997; Clarke and Gaydos, 1998; White and Engelen, 1997; Yeh and Li, 2001), multi-agent systems (Brown et al., 2005; Sanders et al., 1997), updating LC automatically based on change detection using satellite images (Chen et al., 2012; Huang et al., 2017; Jin, et al., 2013; Xian, et al., 2009), multi-temporal remote

http://www.aloki.hu ● ISSN 1589 1623 (Print) ● ISSN 1785 0037 (Online)
DOI: http://dx.doi.org/10.15666/aeer/1703_54495463

sensed imagery (Butt et al., 2015; Fichera et al., 2012; Islam et al., 2018; Nutini et al., 2013), and multispectral airborne laser scanner data (Matikainen et al., 2017). On the other hand, a combination model of RADAR imagery of Sentinel-1 and multispectral imagery of Landsat-8 Operational Land Imager (OLI) has not been performed by other researchers for extracting land covers.

The main objective of this study was to update land cover map using the Google Earth images and the visual interpretation of a combined imagery of RADAR (Sentinel-1) and multispectral (Landsat-8) in Sanandaj County, Kurdistan Province, Iran.

Materials and methods

Description of the study area

Sanandaj County was selected as the study area for this research. The city of Sanandaj, with a population of 432,330, is the most important and the biggest city in Kurdistan Province, Iran. Besides, this scope is located in the Longitudes 46° 24’ 00” E to 47° 19’ 00” E and Latitudes 35° 3’ 00” N to 35° 39’ 00” N (*Fig. 1*).

Moreover, it lies on the border area of Marivan, Divandarreh, Bijar, Dehgolan and Kamyaran Counties. Sanandaj County has a total area of about 3024 km^2. Furthermore, the elevation of the scope ranges from 1450 to 1538 m above the sea level. According to the meteorological department of Iran, the county has the cold and semi-arid climate, but the moderate weather during spring and summer seasons. On the other hand, the maximum and the minimum temperature are about 44 °C and -13.5 °C, in order. While, the average temperature in the spring, summer, autumn and winter are 15.20 °C, 25.20 °C, 10.40 °C and 1.60 °C, respectively (*Table 1*) (Hosseini et al., 2015; Izady, 2015).

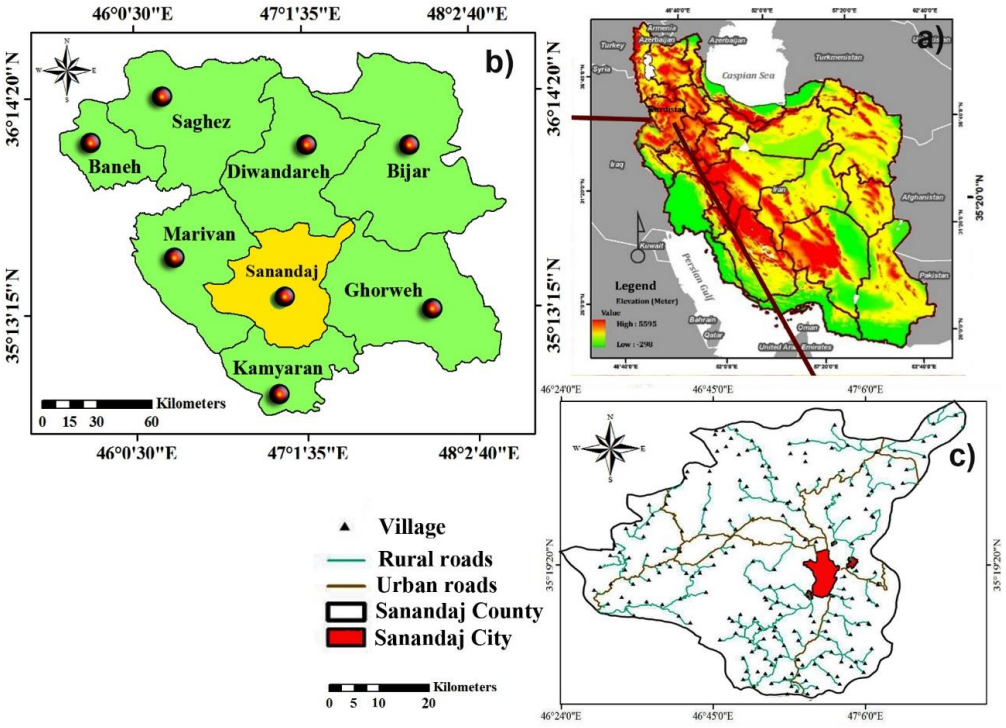

Figure 1. *Geographical location of the study area in a) Northwest of Iran, b) Kurdistan Province, c) Sanandaj County*

http://www.aloki.hu ● ISSN 1589 1623 (Print) ● ISSN 1785 0037 (Online)
DOI: http://dx.doi.org/10.15666/aeer/1703_54495463

Table 1. *Meteorological data applied for the study area*

	Jan	Feb	Mar	Apr	May	Jun	Jul	Aug	Sep	Oct	Nov	Dec	Annual average
Average temperature (°C)	-0.5	0.7	6.4	12.1	16.3	22	26.8	26	20.6	14.7	8	2.3	13
Maximum temperature (°C)	4.8	6.6	13	20	25.3	32.6	44	36.2	32.1	24.3	15.4	8	21.3
Minimum temperature (°C)	-13.5	-5.2	-0.2	4.3	7.4	11.2	16.4	15.6	9.2	5.1	0.6	-3.4	4.6
Monthly average of precipitation (mm)	60.5	65.2	31.4	1	0.7	0.6	1.8	42.8	59.1	91.3	74.5	62.1	491

Image enhancement and visual interpretation

Visual interpretation is highly associated with the knowledge of an applicant about the land covers of an area. Its advantage compared to the automated classification methods is recognizing the dynamic changes more precisely (Kibret et al., 2016; Zhang et al., 2014). The automated classification methods, usually concentrate on the technological approaches, while the visual interpretation is applied for the practical usage (Zhang, et al., 2014).

One of the most important techniques to enhance image's spatial resolution and information is the co-registration and the combination with higher spatial resolution satellite imagery, which improve the visual interpretability of the imagery. However, the enhanced images are normally used for the visual analyses, while the original images are utilized for the automated one (Eastman, 1999; Lillesand et al., 2014).

In the most of remote sensing studies, pre-processing of satellite imageries is undeniable (Belward and Skøien, 2015; Ma et al., 2017). Data pre-processing was applied to provide a radiometrically, atmospherically, spectrally and geometrically corrected imageries. However, based on the study area we acquired 2 Landsat-8 imagery of two different rows of 35 and 36, but the same path of 167, which they were mosaicked and clipped as extend of the study area. Moreover, Sentinel-1 data was acquired for the combination with Landsat-8.

Improvement of the Landsat-8 spatial resolution from 15 m (after pan-sharpening with the 15 m panchromatic band) to 10 m as well as using for the combination model, are among positive points of Sentinel-1 satellite imagery in this study. Using ENVI software, multispectral bands of Landsat-8 imageries of the two rows were pre-

http://www.aloki.hu ● ISSN 1589 1623 (Print) ● ISSN 1785 0037 (Online)
DOI: http://dx.doi.org/10.15666/aeer/1703_54495463

processed and mosaicked. Besides, the thermal band of Landsat-8 and created Normalized Difference Vegetation Index (NDVI) were stacked with the multispectral bands. Furthermore, using SNAP software, Sentinel-1 imagery was pre-processed and clipped as the study area. Moreover, using ENVI software the stacked imagery of multispectral, NDVI and thermal bands (as the slave imagery) was co-registered and stacked with the Sentinel-1 imagery (as the master image). However, the combination of NDVI, RADAR and thermal bands was used for the visual interpretation. At the same time, after extracting the land covers using the Google Earth images with the help of the visual interpretation, the topological errors was fixed in ArcGIS (*Fig. 2*).

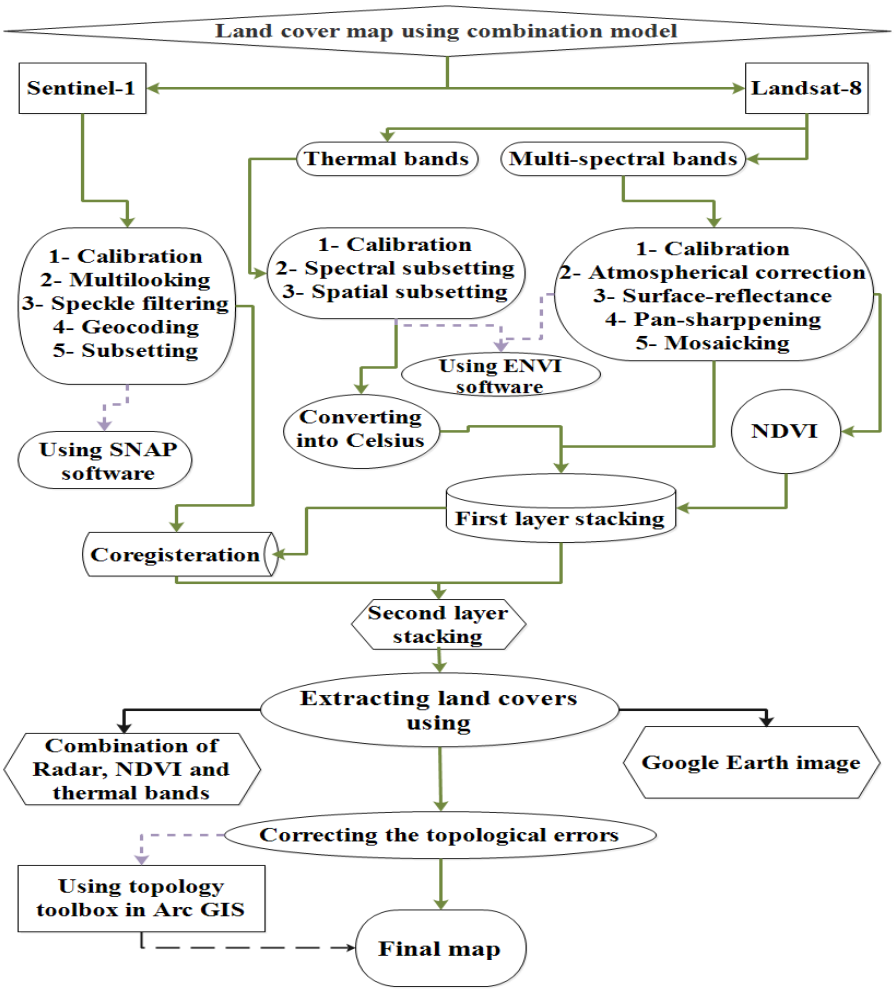

Figure 2. *Methodology of the study*

RADAR, NDVI and thermal bands as a clear combination were interpreted visually, by which the land covers can be differentiated easily. The contrast and brightness level panels were used to adjust the image view to an appropriate level. *Figure 3* illustrates the differences among the land covers by the combined imagery.

Because of the distinguishing in the shape and color, the delineation of the land covers was clear from the combined image's visual interpretation. LCM of the study area was produced from the visual interpretation and digitization using the Google Earth image of the same date in Geographic Information System (GIS).

http://www.aloki.hu ● ISSN 1589 1623 (Print) ● ISSN 1785 0037 (Online)
DOI: http://dx.doi.org/10.15666/aeer/1703_54495463

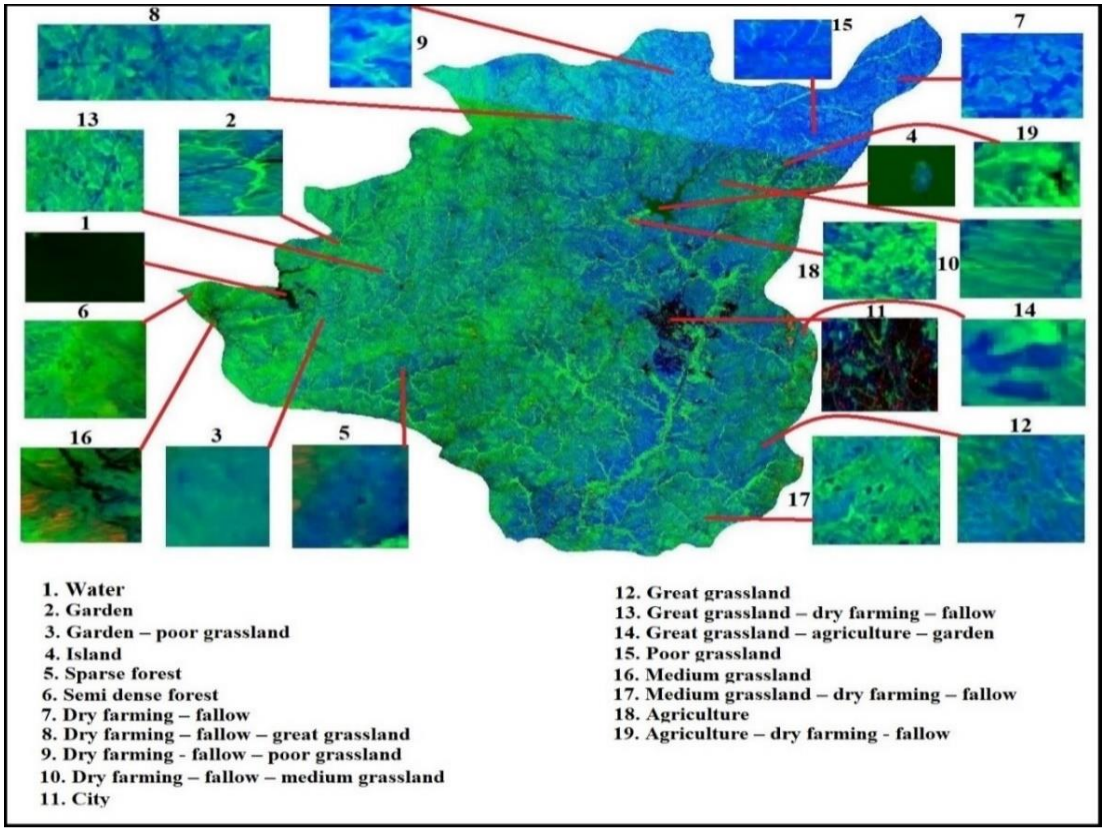

Figure 3. *The combination image of RADAR (Sentinel-1), NDVI (Landsat-8) and thermal bands (Landsat-8)*

Dataset

A pair of Landsat-8 satellite imageries of a same path but two different rows (167-35 and 167-36) were acquired for the study area through https://libra.developementseed.org website. However, these datasets through ENVI software, were corrected and finalized to be co-registered with Sentinel-1 (*Fig. 4*).

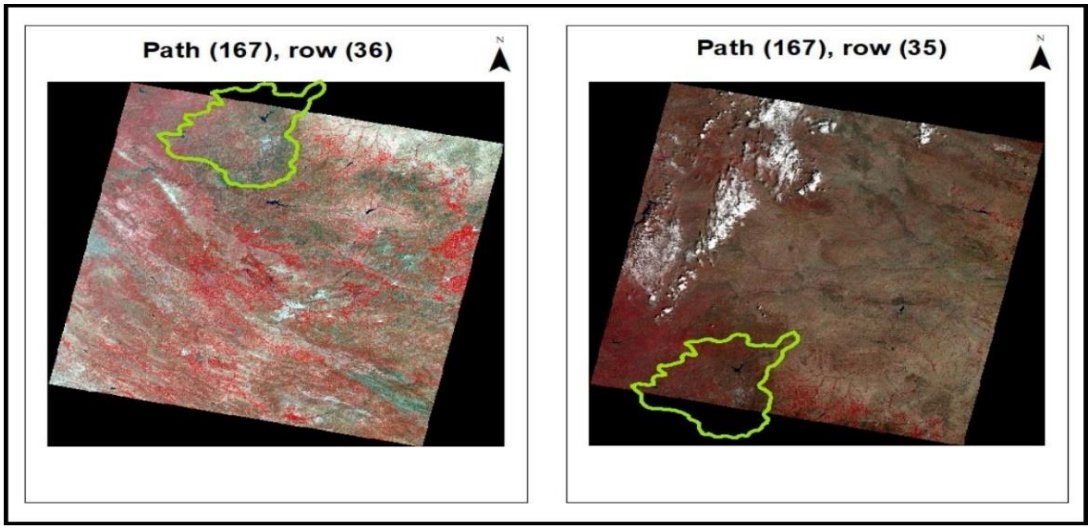

Figure 4. *Landsat-8 images of scope of the study*

http://www.aloki.hu ● ISSN 1589 1623 (Print) ● ISSN 1785 0037 (Online)
DOI: http://dx.doi.org/10.15666/aeer/1703_54495463

Concerned with the Sentinel-1 satellite imagery, based on the study area a scene was downloaded online for free through www.scihub.copernicus.eu website. Using SNAP software, it was prepared for the co-registration process. *Table 2* and *Figure 5* illustrate the technical attributes of the satellite imageries of Sentinel-1 and Landsat-8 and the geographical position of Sentinel-1 data on the study area, respectively.

Table 2. *Technical attributes of the satellite data used in this study*

Characteristics	Sentinel-1	Landsat-8
Type of sensor	SAR	OLI
Spatial resolution	10 m	30 m (multispectral) 15 m (panchromatic)
Temporal resolution	12 days	16 days
Spectral resolution	Single band (C)	9 bands
Date	10/05/2017	11/05/2017
Sensor mode and product type	Interferometry Wide swath (IW) Ground Range Detected (GRD)	

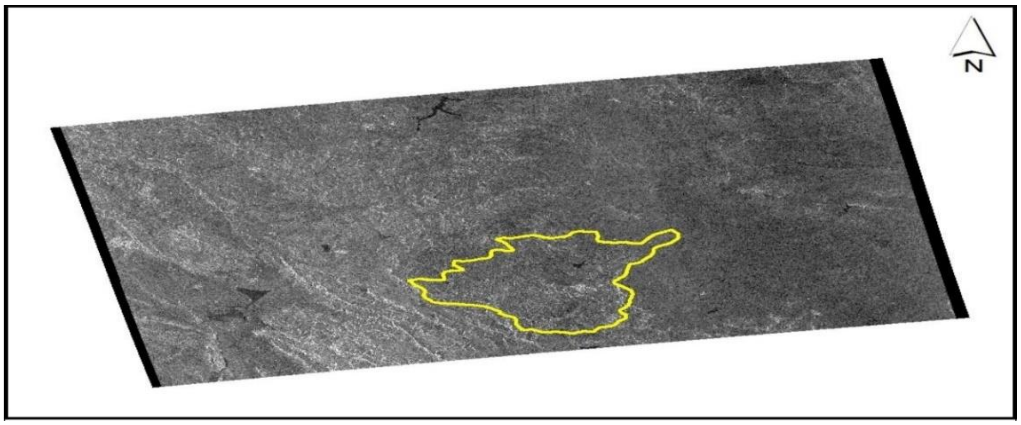

Figure 5. *Sentinel-1 image of scope of the study*

Accuracy assessment

In general, accuracy assessment illustrates the quality of information extracted from remotely sensed data (Alqurashi and Kumar, 2014; Congalton and Green, 2008). The used method for the accuracy assessment in this study was through applying the Google Earth images of the same date. However, it must be considered that using this method only applicable when the researchers have a complete knowledge about the land covers of the study area. For this reason, first the land covers through the visual interpretation of the combined imagery were identified, then all the land covers (polygon by polygon) were digitized and validated through the Google Earth images of the same date.

Results and discussion

The selection of a suitable combination among different bands of satellite imagery is an essential process for the visual interpretation. In order to make a better image visual interpretation, the enhancement technique was fulfilled. In this study, the band

http://www.aloki.hu ● ISSN 1589 1623 (Print) ● ISSN 1785 0037 (Online)
DOI: http://dx.doi.org/10.15666/aeer/1703_54495463

combination of RADAR, NDVI and thermal, was selected as the best combination. An old map was prepared by the Iranian Institute of Water and Soil in 11/05/2010 using Landsat 7 images, ETM^+ sensor with resolution 30 m (multispectral), with row 35 and path 167, which they were mosaicked and clipped as extend of the study area. The extracted images unbalanced machine support model and supervised classification (*Fig. 6*). Because of the big area of Sanandaj County and difficulties in preparation of a new map, this map has been the only available source for citation since 2010.

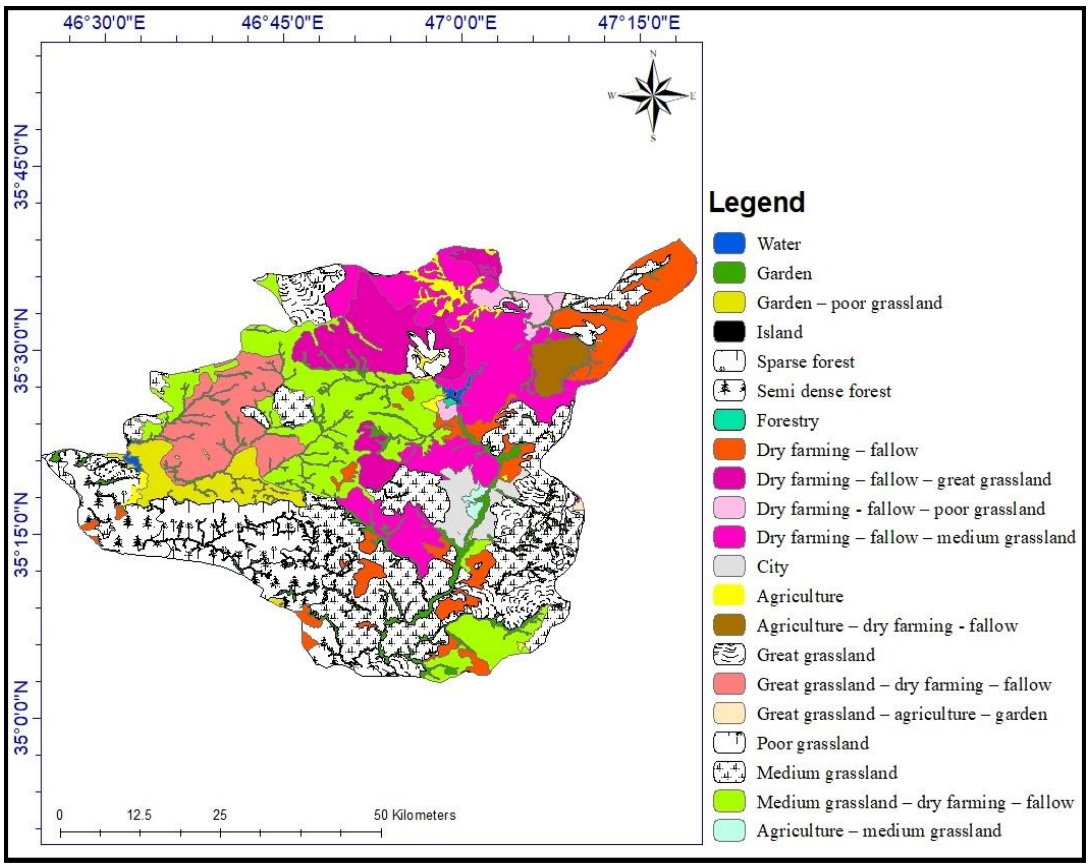

Figure 6. *The land cover map of the study area in the year 2010*

In this study a total number of 19 different land covers ranging from the small to big scales were extracted. However, medium grassland and medium grassland–dry farming–fallow have the biggest area of 497.5818 km^2 and 409.6083 km^2, respectively. Dry farming fallow is the third biggest area with 360.1108 km^2. Moreover, Dry farming–fallow–medium grassland with 259.4949 km^2 is one of the biggest land covers in Sanandaj County. Dry farming–fallow–great grassland, garden and great grassland–dry farming–fallow with 226.3668 km^2, 200.3053 km^2 and 187.1039 km^2, respectively are amongst the substantial land covers of the region. The minimum area of land cover belongs to the island with only 0.119052 km^2. Furthermore, great grassland–agriculture–garden with 1.370851 km^2 is the second smallest area in the study area. The land covers are highlighted in *Figure 7* from the biggest to the smallest.

The final LCM was topologically corrected through the topology toolbox in ArcGIS. However, regardless the applicant patience in digitizing, new digitized layers will be faced with the small topologically errors, which can only be recognized and fixed using

http://www.aloki.hu ● ISSN 1589 1623 (Print) ● ISSN 1785 0037 (Online)
DOI: http://dx.doi.org/10.15666/aeer/1703_54495463

the topology toolbox. Furthermore, in this study, after digitizing a total number of 146 small overlaps and 56 small gaps were identified and corrected one by one through the abovementioned toolbox. *Figure 8* and *Table 3* show the extracted land covers of the study area in the year 2017 and the occurred changes compared with the year of 2010, respectively.

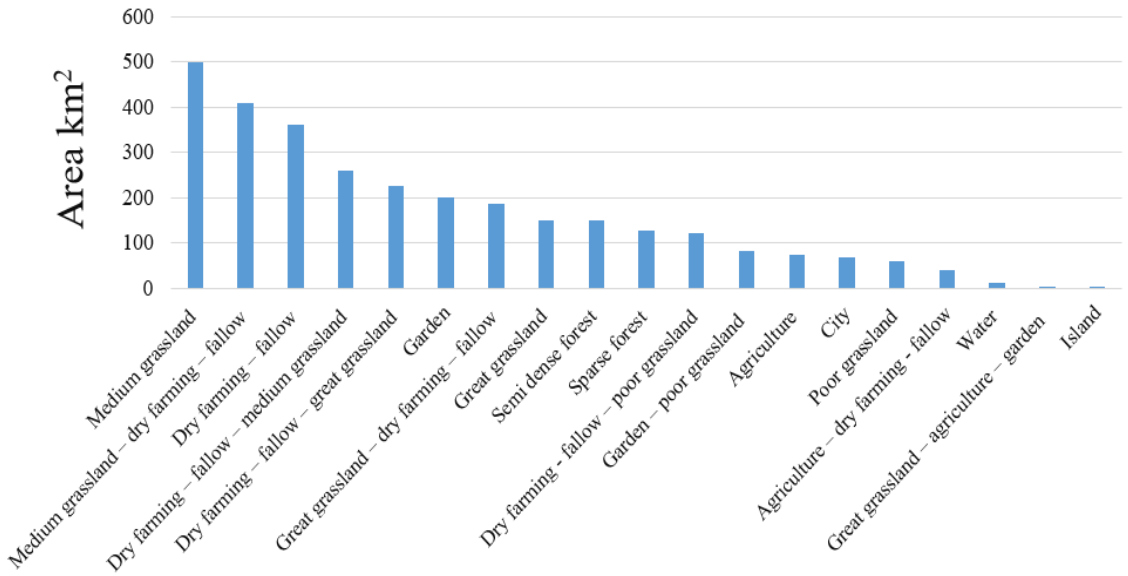

Figure 7. *The land covers and area (km^2) for the study area*

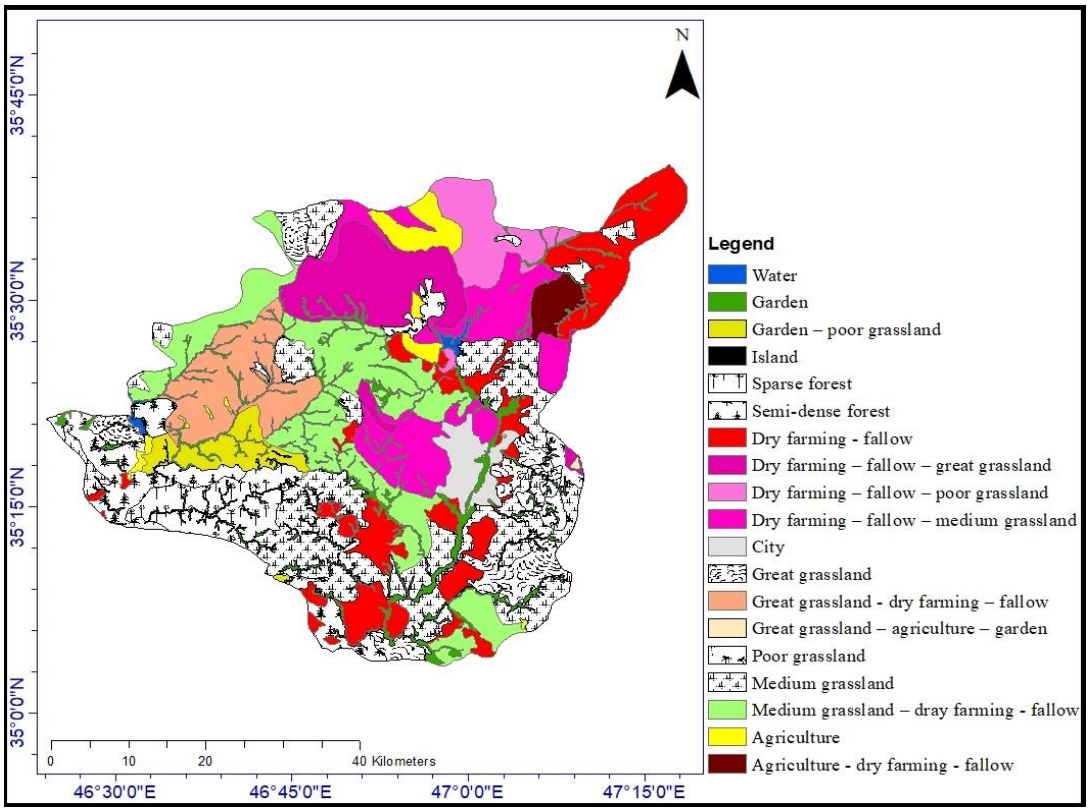

Figure 8. *The land cover map of the study area in the year 2017*

http://www.aloki.hu ● ISSN 1589 1623 (Print) ● ISSN 1785 0037 (Online)
DOI: http://dx.doi.org/10.15666/aeer/1703_54495463

Table 3. *The land cover types and area of each category for the years 2010 and 2017*

No.	Land covers	Area ($km^{2)}$ 2010	Area ($km^{2)}$ 2017
1	Garden	196.561	200.3053
2	water	10.0364	11.61852
3	Garden–poor grassland	101.792	80.78231
4	island	0.238093	0.119052
5	Sparse forest	171.598	128.0167
6	Semi dense forest	171.892	149.8309
7	Forestry	1.4632	Replaced by the dry farming–fallow–poor grassland
8	Dry farming–fallow	230.546	360.1108
9	Dry farming–fallow–great grassland	210.06	226.3668
10	Dry farming–fallow–poor grassland	39.0384	122.2905
11	Dry farming–fallow–medium grassland	378.942	259.4949
12	City	58.6013	67.36704
13	Agriculture	40.9321	73.53178
14	Agriculture–dry farming–fallow	44.0775	39.24857
15	Agriculture–medium grassland	7.68398	Replaced by the city area
16	Great grassland	190.396	150.6862
17	Great grassland–dry farming–fallow	184.367	187.1039
18	Great grassland–agriculture–garden	1.58959	1.370851
19	Poor grassland	41.978	58.51491
20	Medium grassland	543.059	497.5818
21	Medium grassland–dry farming–fallow	399.51	409.6083

Comparing the results of the current study with the results of the research conducted with the Iranian soil and water organization (2010) showed that all the land covers have been faced changes of the small to the large scales. In the year 2017, dry farming–fallow has seen the most considerable changes, where 129.5648 km^2 has been added to its area in comparison with the year 2010. Dry farming–fallow–medium grassland has lost about 119.4471 km^2 of its area by the year 2017. However, because of rising in the water level, the island area decreased to 0.119052 km^2 by 2017 from 0.238093 km^2 in 2010. It is worth indicating that the forestry by the dry farming–fallow–poor grassland and the agriculture-medium grassland by the city area have been replaced.

Extracting land covers using the visual interpretation and the Google Earth is highly associated with the basic knowledge about the study area. However, this technique is very time consuming, but precise and reliable. For example, the water body was recognized from the visual interpretation and digitized through the Google earth image in full zoom, then using ArcGIS converted to the layer format and digitized through the editor toolbox. The obtained results of current study is similar with several previous published studies that investigate land use changes using satellite data in which some will be referred to in this part of the work. Sunar (1998) used five techniques, including: adding, subtracting, dividing, principle component (PCI), and post classification analysis to detect land cover changes in Aykitali, Turkey. He found out that the technique of adding and subtracting images was the most simple among these

http://www.aloki.hu ● ISSN 1589 1623 (Print) ● ISSN 1785 0037 (Online)
DOI: http://dx.doi.org/10.15666/aeer/1703_54495463

techniques, while PCI and post classification analyses showed better results in change detection. Xian et al. (2009) applied Landsat imagery change detection methods for updating the 2001 National Land Cover Database land cover classification to 2006 in several metropolitan areas including Seattle, Washington; San Diego, California; Sioux Falls, South Dakota; Jackson, Mississippi; and Manchester. Results from the five study areas showed that the vast majority of land cover change was captured and updated with overall land cover classification accuracies of 78.32%, 87.5%, 88.57%, 78.36%, and 83.33% for these areas. Shahabi et al. (2012) investigated that green space destruction in urban area using three remote sensing techniques including NDVI, PCA, and post classification methods. To carry out these techniques, Thematic Mapper (TM) and Enhanced Thematic Mapper Plus (ETM+) LANDSAT data within the year 1989 to 2009 were used to recognize land use changes, especially the physical development of the area and its devastating effects on the green space. The result showed that green space has been reduced from 530 ha in 1989 to 198.3 ha in 2009. Butt et al. (2015) applied supervised classification-maximum likelihood algorithm in ERDAS imagine to detection of land cover/land use changes observed in Simly watershed, Pakistan using multispectral satellite data obtained from Landsat 5 and SPOT 5 for the years 1992 and 2012 respectively. The accrued results showed that land cover/land use practices in the study area have altered significantly in 20 years. The land cover/land use shift in the watershed area was evident by the decline in the area of vegetation and water class (38.2% and 74.3% respectively) and augmentation of area covered by classes of settlements (80.1%), Agriculture (163.7%) and barren land (63.3%). Islam et al. (2018) evaluated land use changes of Chunati wildlife sanctuary, Bangladesh from 2005 to 2015 using Landsat TM and Landsat 8 OLI/TIRS images. In the present study Maximum likelihood classification algorithm was used in order to derive supervised land use classification. The obtained results showed that about 256 ha of degraded forest area had been increased within 10 years (2005–2015) and the annual rate of change was 25.56%. Another 159 ha of naturally forested land had been changed to other land uses having an (-) annual rate of change of 15.88%.

Conclusion

In this study, in order to extract the land covers, the satellite imageries of RADAR with multispectral data were combined. The study area lies on an area about 3024 km^2. For this goal, we acquired satellite imageries of Sentinel-1 and Landsat-8 (OLI) for the dates 10/05/2017 and 11/05/2017, respectively (when vegetation coverage is in its best situation). Because of the scope of the study, two Landsat-8 imageries of two different rows (35 and 36) but the same path (167) were downloaded. Moreover, after correcting either Landsat imageries through ENVI Software they were mosaicked as a single image. Sentinel-1 data was corrected using SNAP Software, then as the master image co-registered and stacked with Landsat-8 as the slave image. Besides, RADAR, NDVI and thermal bands were used for the visual interpretation.

Through visual interpretation of the combined imagery with assist of the Google Earth image of the same date, all the land covers were extracted and the topological errors through the topology toolbox in ArcGIS were recognized and corrected. For accuracy assessment the Google Earth image was used, which is a robust way to validate land cover map provided that the researchers have a complete knowledge on the study area. Results illustrate that a total number of 19 different land covers were

http://www.aloki.hu ● ISSN 1589 1623 (Print) ● ISSN 1785 0037 (Online)
DOI: http://dx.doi.org/10.15666/aeer/1703_54495463

recognized and mapped. However, medium grassland, medium grassland–dry farming–fallow and dry farming fallow have the biggest area of 497.5818 km^2, 409.6083 km^2 and 360.1108 km^2, respectively. The smallest area belongs to the island with only 0.119052 km^2, followed by the great grassland–agriculture–garden with 1.370851 km^2. The forestry by the dry farming–fallow–poor grassland and the agriculture-medium grassland by the city area have been replaced.

In this study RADAR imagery of Sentinel-1 (10-m pixel size) was combined with the multispectral data of Landsat-8 (15-m pixel size after pan-sharpening with its panchromatic band), to map the land covers of the study area; however, the combination of the Radar imagery of Sentinel-1 with the multispectral imagery of Sentinel-2 (10-m and 20-m pixel sizes) is highly recommended for such studies in the future.

Acknowledgements. The authors wish to express their sincere thanks to Universiti Teknologi Malaysia (UTM) based on Research University Grant (Q.J130000.2527.17H84) for their financial supports.

REFERENCES

[1] Alqurashi, A. F., Kumar, L. (2014): Land use and land cover change detection in the Saudi Arabian desert cities of Makkah and Al-Taif using satellite data. – Advances in Remote Sensing 3: 106.

[2] Batty, M., Xie, Y. (1994): From cells to cities. – Environment and Planning B: Planning and Design 21: S31-S48.

[3] Batty, M., Xie, Y. (1997): Possible urban automata. – Environment and Planning B: Planning and Design 24: 175-192.

[4] Belal, A., Moghanm, F. (2011): Detecting urban growth using remote sensing and GIS techniques in Al Gharbiya governorate, Egypt. – The Egyptian Journal of Remote Sensing and Space Science 14: 73-79.

[5] Belward, A. S., Skøien, J. O. (2015): Who launched what, when and why: trends in global land-cover observation capacity from civilian earth observation satellites. – ISPRS Journal of Photogrammetry and Remote Sensing 103: 115-128.

[6] Boori, M. S., Voženílek, V., Choudhary, K. (2015): Land use/cover disturbance due to tourism in Jeseníky Mountain, Czech Republic: a remote sensing and GIS based approach. – The Egyptian Journal of Remote Sensing and Space Science 18: 17-26.

[7] Brown, D. G., Page, S., Riolo, R., Zellner, M., Rand, W. (2005): Path dependence and the validation of agent-based spatial models of land use. – International Journal of Geographical Information Science 19: 153-174.

[8] Butt, A., Shabbir, R., Ahmad, S. S., Aziz, N. (2015): Land use change mapping and analysis using Remote Sensing and GIS: A case study of Simly watershed, Islamabad, Pakistan. – The Egyptian Journal of Remote Sensing and Space Science 18: 251-259.

[9] Chen, G. P., He, C., Pu, R., Shi, P. (2003): Land-use/land-cover change detection using improved change-vector analysis. – Photogrammetric Engineering & Remote Sensing 69: 369-379.

[10] Chen, X., Chen, J., Shi, Y., Yamaguchi, Y. (2012): An automated approach for updating land cover maps based on integrated change detection and classification methods. – ISPRS Journal of Photogrammetry and Remote Sensing 71: 86-95.

[11] Clarke, K. C., Gaydos, L. J. (1998): Loose-coupling a cellular automaton model and GIS: long-term urban growth prediction for San Francisco and Washington/Baltimore. – International Journal of Geographical Information Science 12: 699-714.

[12] Congalton, R. G., Green, K. (2008): Assessing the Accuracy of Remotely Sensed Data: Principles and Practices. – CRC, Boca Raton, FL.

http://www.aloki.hu ● ISSN 1589 1623 (Print) ● ISSN 1785 0037 (Online)
DOI: http://dx.doi.org/10.15666/aeer/1703_54495463

[13] Eastman, J. R. (1999): Guide to GIS and Image Processing (Vol. 1). – Clark Labs, Clark University, USA.
[14] El-Kawy, O. A., Rød, J., Ismail, H., Suliman, A. (2011): Land use and land cover change detection in the western Nile delta of Egypt using remote sensing data. – Applied Geography 31: 483-494.
[15] Fichera, C. R., Modica, G., Pollino, M. (2012): Land cover classification and change-detection analysis using multi-temporal remote sensed imagery and landscape metrics. – European Journal of Remote Sensing 45: 1-18.
[16] Grecchi, R. C., Gwyn, Q. H. J., Bénié, G. B., Formaggio, A. R., Fahl, F. C. (2014): Land use and land cover changes in the Brazilian Cerrado: A multidisciplinary approach to assess the impacts of agricultural expansion. – Applied Geography 55: 300-312.
[17] Halmy, M. W. A., Gessler, P. E., Hicke, J. A., Salem, B. B. (2015): Land use/land cover change detection and prediction in the north-western coastal desert of Egypt using Markov-CA. – Applied Geography 63: 101-112.
[18] Hansen, M. C., Loveland, T. R. (2012): A review of large area monitoring of land cover change using Landsat data. – Remote Sensing of Environment 122: 66-74.
[19] Homer, C., Huang, C., Yang, L., Wylie, B., Coan, M. (2004): Development of a 2001 national land-cover database for the United States. – Photogrammetric Engineering & Remote Sensing 70: 829-840.
[20] Hosseini, G., Teymouri, P., Shahmoradi, B., Maleki, A. (2015): Determination of the concentration and composition of PM10 during the Middle Eastern dust storms in Sanandaj, Iran. – Journal of Research in Health Sciences 15: 182-188.
[21] Huang, S., Ramirez, C., Kennedy, K., Mallory, J., Wang, J., Chu, C. (2017): Updating land cover automatically based on change detection using satellite images: case study of national forests in Southern California. – GIScience & Remote Sensing 54: 495-514.
[22] Islam, K., Jashimuddin, M., Nath, B., Nath, T. K. (2018): Land use classification and change detection by using multi-temporal remotely sensed imagery: the case of Chunati wildlife sanctuary, Bangladesh. – The Egyptian Journal of Remote Sensing and Space Science 21: 37-47.
[23] Izady, M. (2015): The Kurds: A Concise History and Fact Book. – Taylor & Francis, New York.
[24] Jin, S., Yang, L., Danielson, P., Homer, C., Fry, J., Xian, G. (2013): A comprehensive change detection method for updating the National Land Cover Database to circa 2011. – Remote Sensing of Environment 132: 159-175.
[25] Kibret, K. S., Marohn, C., Cadisch, G. (2016): Assessment of land use and land cover change in South Central Ethiopia during four decades based on integrated analysis of multi-temporal images and geospatial vector data. – Remote Sensing Applications: Society and Environment 3: 1-19.
[26] Kumar, K., Kumar, V., Kumar, D. (2016): Land use and land cover change detection ingagas river valley watershed using remote sensing and GIS. – International Journal of Research in Engineering and Applied Sciences 6: 31-37.
[27] Lausch, A., Herzog, F. (2002): Applicability of landscape metrics for the monitoring of landscape change: issues of scale, resolution and interpretability. – Ecological Indicators 2: 3-15.
[28] Li, X., Yeh, A. G.-O. (2002): Neural-network-based cellular automata for simulating multiple land use changes using GIS. – International Journal of Geographical Information Science 16: 323-343.
[29] Li, Y., Cao, Z., Long, H., Liu, Y., Li, W. (2017): Dynamic analysis of ecological environment combined with land cover and NDVI changes and implications for sustainable urban–rural development: the case of Mu Us Sandy Land, China. – Journal of Cleaner Production 142: 697-715.
[30] Lillesand, T., Kiefer, R. W., Chipman, J. (2014): Remote Sensing and Image Interpretation. – John Wiley & Sons, Hoboken.

http://www.aloki.hu ● ISSN 1589 1623 (Print) ● ISSN 1785 0037 (Online)
DOI: http://dx.doi.org/10.15666/aeer/1703_54495463

[31] Liu, T., Yang, X. (2015): Monitoring land changes in an urban area using satellite imagery, GIS and landscape metrics. – Applied Geography 56: 42-54.
[32] López, E., Bocco, G., Mendoza, M., Duhau, E. (2001): Predicting land-cover and land-use change in the urban fringe: a case in Morelia city, Mexico. – Landscape and Urban Planning 55: 271-285.
[33] Loveland, T., Sohl, T., Stehman, S., Gallant, A., Sayler, K., Napton, D. (2002): A strategy for estimating the rates of recent United States land-cover changes. – Photogrammetric Engineering & Remote Sensing 68: 1091-1099.
[34] Lunetta, R. S., Knight, J. F., Ediriwickrema, J., Lyon, J. G., Worthy, L. D. (2006): Land-cover change detection using multi-temporal MODIS NDVI data. – Remote Sensing of Environment 105: 142-154.
[35] Ma, L., Li, M., Ma, X., Cheng, L., Du, P., Liu, Y. (2017): A review of supervised object-based land-cover image classification. – ISPRS Journal of Photogrammetry and Remote Sensing 130: 277-293.
[36] Matikainen, L., Karila, K., Hyyppä, J., Litkey, P., Puttonen, E., Ahokas, E. (2017): Object-based analysis of multispectral airborne laser scanner data for land cover classification and map updating. – ISPRS Journal of Photogrammetry and Remote Sensing 128: 298-313.
[37] Myint, S. W., Gober, P., Brazel, A., Grossman-Clarke, S., Weng, Q. (2011): Per-pixel vs. object-based classification of urban land cover extraction using high spatial resolution imagery. – Remote Sensing of Environment 115: 1145-1161.
[38] Nutini, F., Boschetti, M., Brivio, P., Bocchi, S., Antoninetti, M. (2013): Land-use and land-cover change detection in a semi-arid area of Niger using multi-temporal analysis of Landsat images. – International journal of remote sensing 34: 4769-4790.
[39] Rawat, J., Kumar, M. (2015): Monitoring land use/cover change using remote sensing and GIS techniques: a case study of Hawalbagh block, district Almora, Uttarakhand, India. – The Egyptian Journal of Remote Sensing and Space Science 18: 77-84.
[40] Rawat, J., Biswas, V., Kumar, M. (2013): Changes in land use/cover using geospatial techniques: a case study of Ramnagar town area, district Nainital, Uttarakhand, India. – The Egyptian Journal of Remote Sensing and Space Science 16: 111-117.
[41] Sanders, L., Pumain, D., Mathian, H., Guérin-Pace, F., Bura, S. (1997): SIMPOP: a multiagent system for the study of urbanism. – Environment and Planning B: Planning and Design 24: 287-305.
[42] Shahabi, H., Ahmad, B. B., Mokhtari, M. H., Zadeh, M. A. (2012): Detection of urban irregular development and green space destruction using normalized difference vegetation index (NDVI), principal component analysis (PCA) and post classification methods: a case study of Saqqez City. – International Journal of Physical Sciences 7: 2587-2595.
[43] Sunar, F. (1998): An analysis of changes in a multi-date data set: a case study in the Ikitelli area, Istanbul, Turkey. – International Journal of Remote Sensing 19: 225-235.
[44] Theobald, D. M., Hobbs, N. T. (1998): Forecasting rural land-use change: a comparison of regression-and spatial transition-based models. – Geographical and Environmental Modelling 2: 65-82.
[45] White, R., Engelen, G. (1997): Cellular automata as the basis of integrated dynamic regional modelling. – Environment and Planning B: Planning and Design 24: 235-246.
[46] Wu, F., Yeh, A. G.-O. (1997): Changing spatial distribution and determinants of land development in Chinese cities in the transition from a centrally planned economy to a socialist market economy: a case study of Guangzhou. – Urban Studies 34: 1851-1879.
[47] Xian, G., Crane, M. (2005): Assessments of urban growth in the Tampa Bay watershed using remote sensing data. – Remote Sensing of Environment 97: 203-215.
[48] Xian, G., Homer, C., Fry, J. (2009): Updating the 2001 National Land Cover Database land cover classification to 2006 by using Landsat imagery change detection methods. – Remote Sensing of Environment 113: 1133-1147.

http://www.aloki.hu ● ISSN 1589 1623 (Print) ● ISSN 1785 0037 (Online)
DOI: http://dx.doi.org/10.15666/aeer/1703_54495463

[49] Yeh, A. G.-O., Li, X. (2001): A constrained CA model for the simulation and planning of sustainable urban forms by using GIS. – Environment and Planning B: Planning and Design 28: 733-753.
[50] Zhang, Z., Wang, X., Zhao, X., Liu, B., Yi, L., Zuo, L., Hu, S. (2014): A 2010 update of National Land Use/Cover Database of China at 1: 100000 scale using medium spatial resolution satellite images. – Remote Sensing of Environment 149: 142-154.
[51] Zhu, Z., Woodcock, C. E. (2014): Continuous change detection and classification of land cover using all available Landsat data. – Remote Sensing of Environment 144: 152-171.

http://www.aloki.hu ● ISSN 1589 1623 (Print) ● ISSN 1785 0037 (Online)
DOI: http://dx.doi.org/10.15666/aeer/1703_54495463